ARTICLE

OBC
www.rsc.org/obc

Electrophilic and oxidative chemistry of pyrene and its non-alternant isomers: theoretical (DFT, GIAO-NMR, NICS) study of protonation carbocations and oxidation dications from pyrene, azupyrene (dicyclopenta[*ef*,*kl*]heptalene) and dicyclohepta[*ed*,*gh*]-pentalene†

Takao Okazaki[a,b] and Kenneth K. Laali*[b]

[a] *Department of Energy and Hydrocarbon Chemistry, Kyoto University, Kyoto, Japan*

[b] *Department of Chemistry, Kent State University, Kent, OH, 44242, USA*

Received 5th April 2004, Accepted 15th June 2004
First published as an Advance Article on the web 14th July 2004

Mono- and diprotonated carbocations and the two-electron oxidation dications derived from parent pyrene **1** and its nonalternant isomers "azupyrene" (dicyclopenta[*ef*,*kl*]heptalene) (DCPH) **2** and dicyclohepta[*ed*,*gh*]pentalene (DCHP) **3** were studied by DFT at the B3LYP/6-31G(d) level. The most likely site(s) for mono- and diprotonation were determined based on relative arenium ion energies and the structures of the energetically most favored carbocations were determined by geometry optimization. The NMR chemical shifts for the protonated mono- and dications and the oxidation dications were computed by GIAO-NMR at the B3LYP/6-31G(d)//B3LYP/6-31G(d) level and their charge delocalization paths were deduced based on magnitude of the computed $\Delta\delta^{13}$C values and the NPA-derived changes in charges. Relative aromaticity/antiaromaticity in various rings in the energetically favored mono- and dications was estimated *via* NICS and ΔNICS. Calculated NMR chemical shift data for $\mathbf{1H}^+$ and $\mathbf{1}^{2+}$ were compared with the available experimental NMR values. The available data on chemical and physical properties of DCPH **2** and DCHP **3** are extremely limited and biological activity data are non-existent. The present study provides the first glance into their carbocations and oxidation dications, while augmenting and reinforcing the previous stable ion data on the pyrenium cations.

Introduction

The pyrene skeleton **1** is an important building block and constituent in PAH chemistry and in structure/bioactivity studies (Fig. 1). Whereas parent **1** is biologically inactive, some of its substituted analogs such as 1-nitro- and 2-nitropyrenes are mutagenic, whereas 4-nitropyrene is both mutagenic and tumorigenic.[1] The benzannelated derivative benzo[*a*]pyrene BaP with a bay-region is a strong carcinogen, while the distorted dibenzannelated derivative dibenzo[*al*]pyrene with a fjord-region is extremely potent.[2]

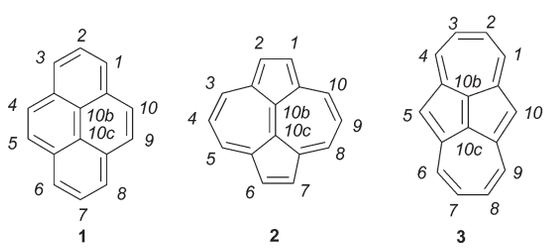

Fig. 1 Pyrene (**1**), dicyclopenta[*ef*,*kl*]heptalene "azupyrene" (**2**), and dicyclohepta[*ed*,*gh*]pentalene (**3**).

Dicyclopenta[*ef*,*kl*]heptalene (DCPH) **2**, more commonly known as "azupyrene", and dicyclohepta[*ed*,*gh*]pentalene (DCHP) **3** are the non-alternant isomers of **1** (Fig. 1).[3–5] They constitute 14π-Hückel aromatic peripheral systems perturbed by a central double bond. This is borne out by their X-ray structures, showing that the central double bonds are noticeably short (1.333 Å for **2** and 1.354 Å for **3**).[5b,6]

The synthesis of **2** and the modifications thereof were reported by Anderson,[3,4] Jutz,[7] and Hafner[8] and their associates, whereas **3** was synthesized by Vogel *et al.*[5] Representative electrophilic aromatic substitution data (namely acetylation, trifluroacetylation, and nitration) are available on **2** and some of its C(1) and C(4) substituted derivatives, showing (for parent **2**) predominant substitution at C(1) (although in some cases products of C(4) substitution have also been isolated).[4] With the C(1) substituted derivatives, further substitution occurred (in most cases) at C(2), C(6), and C(7).[4] Further acetylation of the 4-COMe derivative and further nitration of the 4-NO_2 derivative were reported to result in substitution at C(1) and C(2).[4]

Hydrocarbon **3** is protonated in TFA at C(5) to give a stable carbenium ion for which Vogel reported a room temperature proton spectrum.[5a] Previous theoretical studies on **2** and **3** were limited to HMO and MNDO calculations.[5,9]

An additional noteworthy point is that under appropriate conditions the central bond **2** is capable of undergoing nucleophilic attack. Quenching of the resulting monoanionic intermediates with electrophiles led to the synthesis of various bridged [14]annulenes.[10] Nucleophile addition is a LUMO-controlled process because the largest LUMO coefficient is at the central bond (from HMO).[10]

Whereas stable ion NMR data are available on various protonated and sulfinylated pyrenium cations[11,12] and several examples of persistent two-electron oxidation dications have also been reported,[13,14] no such data are available for **2** and **3**. Furthermore, no comparative biological activity data are hitherto available for **2–3** or their derivatives.

Formation of PAH-DNA adducts, a key-step in tumor initiating activity of PAHs, occurs either *via* the diol-epoxide pathway or by a SET mechanism involving PAH radical cations.[15] Depending on the PAH structure, the former path in many instances involves carbocations as key electrophiles.[16] Once intercalated into DNA, the generated metabolic electrophiles form stable and depurinating adducts.[15]

† Electronic supplementary information (ESI) available: Table S1: Electronic energies (*E*), zero point energies (ZPE) and Gibbs free energies (*G*) obtained from DFT calculations for the studied molecules and cations at B3LYP/6-31G(d) level. Figs. S1, S8 and S10 and Tables S2–S14: Optimized structures and Cartesian coordinates for **1**, $\mathbf{1aH}^+$, $\mathbf{1bH_2}^{2+}$, $\mathbf{1}^{2+}$, **2**, $\mathbf{2aH}^+$, $\mathbf{2aH_2}^{2+}$, $\mathbf{2}^{2+}$, **3**, $\mathbf{3cH}^+$, $\mathbf{3eH_2}^{2+}$ and $\mathbf{3}^{2+}$. Figs. S2, S3 and S4: Computed ^{13}C NMR chemical shifts and NPA-derived charges for $\mathbf{1aH}^+$, $\mathbf{1_2}^{2+}$ and $\mathbf{1}^{2+}$. Fig. S5: Experimental ^{13}C NMR chemical shifts for $\mathbf{1aH}^+$ and $\mathbf{1}^{2+}$. Figs. S6, S7, and S12: HOMO–LUMO forms in the oxidation dications. Figs. S9 and S11: Bond-lengths in X-ray derived and computed structures for **2** and **3**. See http://www.rsc.org/suppdata/ob/b4/b405009f/

DOI: 10.1039/b405009f

In the case of BaP-diol-epoxide (BPDE), it was shown that rapid formation of an intercalated complex is followed by rate determining protonation to give an intercalated triolcarbenium ion (Fig 2).[17]

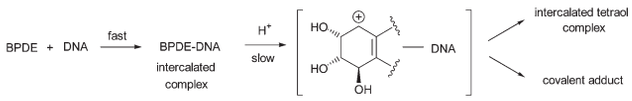

Fig. 2 Intercalation into DNA and carbocation formation.

Facile carbocation formation from **2** and **3** coupled to feasibility of nucleophilic addition to the central bond render these substrates interesting for both stable ion and DNA binding studies. The present study, which represents our first step in this direction, focuses on relative carbocation energies, geometries, charge delocalization modes in the resulting carbocations and in the oxidation dications (gauged *via* magnitude of $\Delta\delta^{13}$C values by GIAO-NMR and the NPA-derived changes in charges), and on the relative aromaticity/antiaromaticity in various rings in these systems (gauged *via* NICS and ΔNICS).

Results and discussion

DFT calculations

Structures were optimized using molecular point groups shown in Table S1 of the electronic supplementary information (ESI) by the density functional theory (DFT) method at B3LYP/6-31G(d) level using the Gaussian 98 package.[18] Computed geometries were verified by frequency calculations. Furthermore, global minima were checked by manually changing initial geometries and by comparing the resulting optimized structures and their energies. NMR chemical shifts and NICS[19] values were calculated by the GIAO[20] methods at the B3LYP/6-31G(d)//B3LYP/6-31G(d) level. NMR chemical shifts were referenced to TMS (GIAO magnetic shielding tensor = 183.7642 ppm) calculated with a molecular symmetry of T_d at the same level of theory. NICS values were measured at the ring centroid. Table S1 (in the ESI) summarizes the total energies (*E*), zero point energies (ZPE), and Gibbs free energies (*G*) for the neutral substrates, mono- and diprotonated cations and the oxidation dications.

Pyrene (1). DFT optimized structures of **1** (C_s symmetry; this geometry is almost the same as the D_{2h} symmetrical structure), **1aH**$^+$ (C_s), **1bH**$^+$ (C_{2v}), **1cH**$^+$ (C_s), **1aH$_2$**$^{2+}$ (C_{2v}), **1bH$_2$**$^{2+}$ (C_s), **1cH$_2$**$^{2+}$ (C_{2h}), **1dH$_2$**$^{2+}$ (C_{2v}), **1eH$_2$**$^{2+}$ (C_s), **1fH$_2$**$^{2+}$ (C_2), **1gH$_2$**$^{2+}$ (C_{2h}), **1hH$_2$**$^{2+}$ (C_{2v}) and **1iH$_2$**$^{2+}$ (C_1) were calculated to be minima (see Fig. 3). Whereas the singlet dication **1**$^{2+}$ (C_s), and the triplet diradical dication **1**$^{2+}$ (C_s) were both calculated to be minima, the former is considerably more stable (by 14.6 kcal mol^{-1}).

In agreement with earlier stable ion work,[12] the most stable arenium ion among monoprotonated pyrenes is **1aH**$^+$, which is protonated at the C(1) position (the α-position). Cation **1cH**$^+$ (αβ-protonated) lies 10.5 kcal mol^{-1} higher (early PI-DEWAR calculations gave a value 8.8 kcal mol^{-1})[21], whereas **1bH**$^+$ (β-protonated) lies 15.0 kcal mol^{-1} above **1aH**$^+$ (20.5 kcal mol^{-1} higher by PI-DEWAR method!).[21]

Persistent diprotonated pyrenium dications have not been observed under stable ion conditions,[11,12] To get a sense for relative arenium ion energies, all possible protonation dications were computed in the context of present study. Interestingly, based on DFT, the 1,4-diprotonated dication **1bH$_2$**$^{+2}$ is the most favored, followed closely by **1iH$_2$**$^{+2}$ (1,2-), **1dH$_2$**$^{+2}$ (1,8-), **1eH$_2$**$^{+2}$ (1,10-), **1gH$_2$**$^{+2}$ (4,9-), **1cH$_2$**$^{+2}$ (1,6-), and **1hH$_2$**$^{+2}$ (4,10-), whereas **1aH$_2$**$^{+2}$ (1,3-attack) does not compete well.

Optimized geometries for **1**, **1aH**$^+$, **1bH$_2$**$^{2+}$ and **1**$^{2+}$ are shown in Fig. S1 for comparison. The largest changes in bond-lengths in **1aH**$^+$ are for the C(1)/C(2) and C(1)/C(10a) bonds which are noticeably longer due to rehybridization at C(1). A reasonable overall bond-alternation scheme (shorter/longer relative to **1**) can be deduced for **1aH**$^+$. This feature is more pronounced in the dication

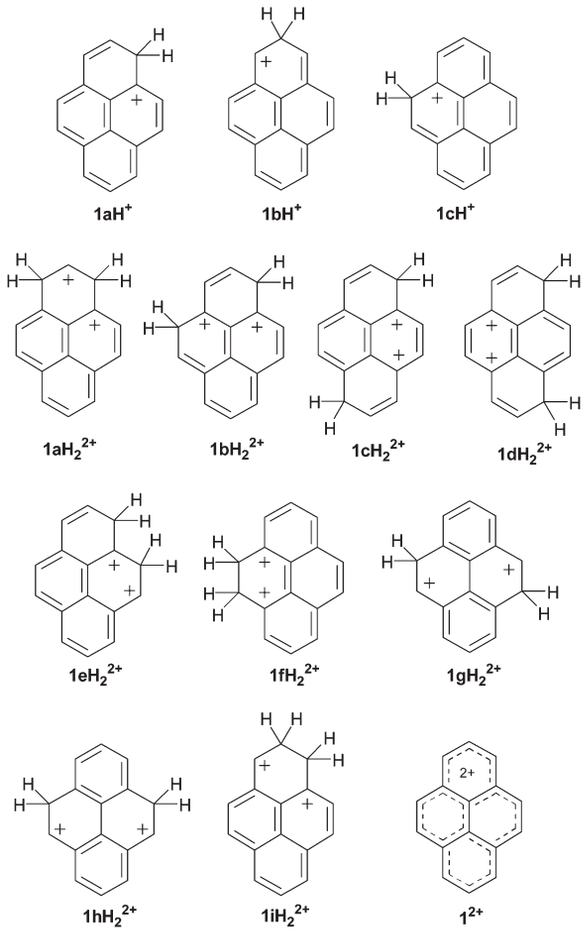

Fig. 3 Protonated monopyrenium ions (**1aH**$^+$**–1cH**$^+$), diprotonated pyrenium dication (**1aH$_2$**$^{2+}$**–1iH$_2$**$^{2+}$) and pyrene oxidation dication (**1**$^{2+}$).

1^{2+}. Interestingly, for these cations, the C(10b)/C(10c) bond-lengths (*central double bonds*) are nearly constant.

The computed GIAO-NMR data, and the NPA-derived charges (and changes in carbon charges) relative to parent hydrocarbon **1**, as well as the NPA-derived overall charges over CH units for **1aH**$^+$ and **1**$^{2+}$ are gathered in Figures S2–S4. For comparison, the stable ion ^{13}C NMR chemical shifts[11] for **1aH**$^+$ and **1**$^{2+}$ are also gathered (in Fig. S5).

Even though for both cations, GIAO slightly underestimates the chemical shifts (between 5–15 ppm in the case of **1aH**$^+$ and 11–16 ppm in the case of **1**$^{2+}$), the overall agreement, especially in deducing overall charge delocalization paths based on $\Delta\delta^{13}$C values, is very good. This can be further illustrated *via* Fig. 4 in which the GIAO-derived chemical shifts for **1aH**$^+$ and **1**$^{2+}$ are plotted against the experimental data. Fig. 4a illustrates the computed data *versus* experiment, using the $\Delta\delta^{13}$C values.

Pyrenium ion **1aH**$^+$ shows a distinct and continuous charge alternation path throughout the entire periphery. A similar charge alternation is observed in **1bH$_2$**$^{2+}$ but with larger $\Delta\delta^{13}$C values (Fig S3). Positive charge in the singlet dication is most strongly localized at the α-positions. Similar overall charge delocalization paths may be arrived at based on the NPA-derived changes of charges (see Fig. S2–S4).

The NICS and ΔNICS values are gathered in Fig 5. For **1aH**$^+$ and **1bH$_2$**$^{2+}$ the individual rings are still aromatic/borderline aromatic. For the singlet **1**$^{2+}$ there is a strong positive shift upon two-electron oxidation indicative of anti-aromaticity, and this is consistent with paratropicity in the 12π-perimeter dication which was previously deduced based on NMR.[13,14] Interestingly, NICS suggests that the less stable triplet dication should be aromatic.

Finally, the HOMO–LUMO forms of for the singlet **1**$^{2+}$ are illustrated in Fig. S6, showing that the central double bond does not contribute to HOMO.

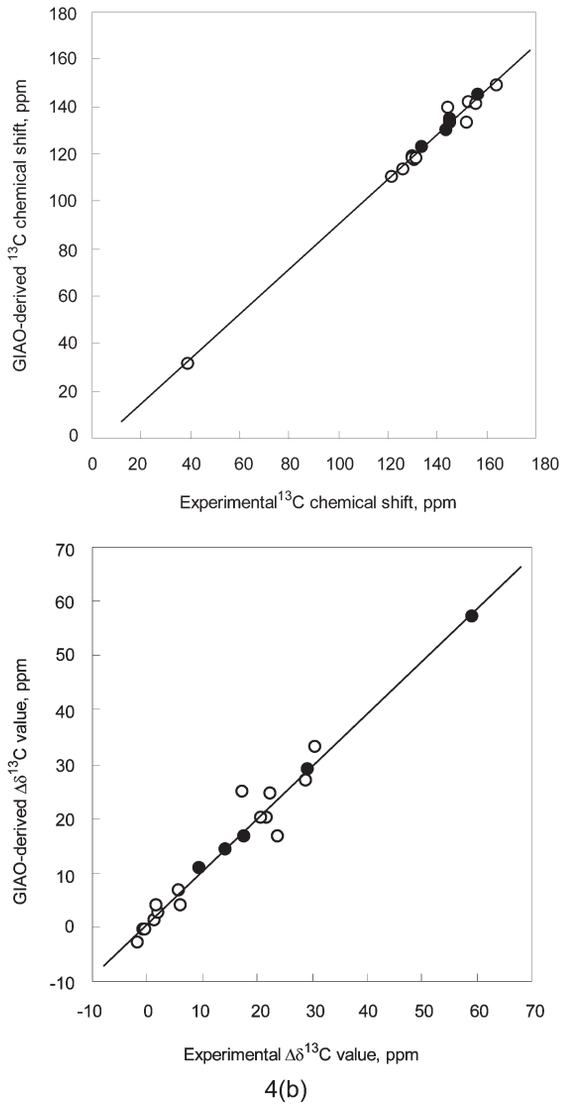

Fig. 4 Plot of experimental $\Delta\delta^{13}$C value vs GIAO-derived $\Delta\delta^{13}$C value for **1aH**$^+$ (○) and **1**$^{2+}$ (●).

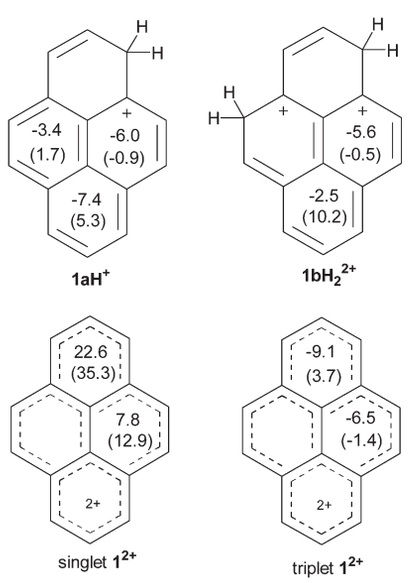

Fig. 5 NICS(0) for **1aH**$^+$, **1bH$_2$**$^{2+}$ and singlet and triplet **1**$^{2+}$ (ΔNICS values relative to those of **1** in parentheses).

Dicyclopenta[*ef*,*kl*]heptalene (2). The DFT optimized structures of **2** with C_s symmetry (this geometry is almost the same as the D_{2h} symmetrical structure), **2aH**$^+$ (protonation at C-1) with C_s symmetry, **2bH**$^+$ (protonation at C-2a) with C_1 symmetry, **2cH**$^+$ (protonation at C-3) with C_1 symmetry (the C_s symmetrical carbocation had the same energy), and **2dH**$^+$ (protonation at C-4) with C_s symmetry were found to be minima and the most stable (see Fig 6 and Table S1 of the ESI).

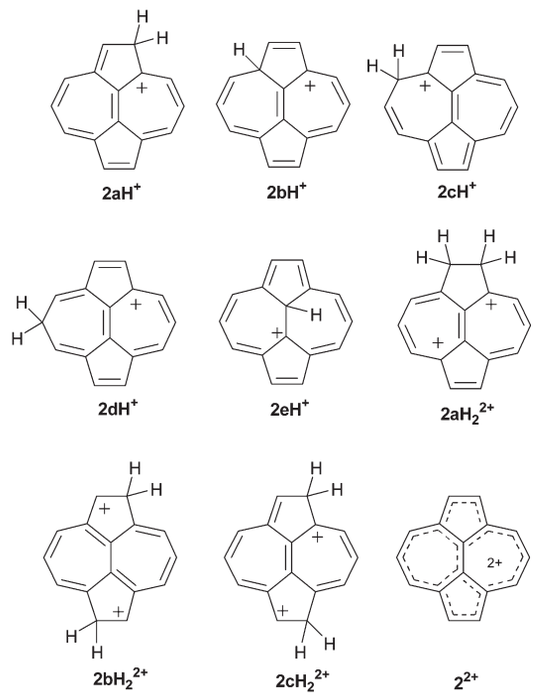

Fig. 6 Protonated azupyrenium ions **2aH**$^+$–**2eH**$^+$, diprotonated azupyrenium dications **2aH$_2$**$^{2+}$–**2cH$_2$**$^{2+}$ and the oxidation dication **2**$^{2+}$.

Among various possible dications, **2aH$_2$**$^{2+}$ (protonated at C-1 and C-2) with C_{2v} symmetry, and the singlet oxidation dication **2**$^{2+}$ with C_s symmetry (this geometry is almost the same as the D_{2h} symmetrical structure) were calculated to be minima (Fig 6 and Table S1 of the ESI).

Based on relative carbocation energy data for azupyrene, protonation at C(1) (five-membered ring) is energetically most favored and this is consistent with the available electrophilic aromatic substitution data on **2** (see introduction). The next best candidate is **2dH**$^+$ which is 3.5 kcal mol^{-1} less stable. For diprotonation, the second protonation is more likely to occur in the same five-membered ring to give **2aH$_2$**$^{2+}$ than in the opposite five-membered ring. This pattern generates a bis-tropylium dication.

The singlet dication of azupyrene was computed to be *ca.* 4 kcal mol^{-1} more stable than the triplet diradical dication. The HOMO–LUMO forms in singlet **2**$^{2+}$ are illustrated in Fig. S7 of the ESI. The HOMO has large coefficients at C(1)/C(2) and C(6)/C(7), and similar to **1**$^{2+}$, the central double bond does not contribute to HOMO in **2**$^{2+}$.

Charge delocalization modes deduced based on magnitude of GIAO $\Delta\delta^{13}$C values in the energetically most favored monocation **2aH**$^+$, diprotonated dication **2aH$_2$**$^{2+}$ and the oxidation dication **2**$^{2+}$ are sketched in Fig 7 for comparison. The NPA-derived charges and changes in charges are also included.

Whereas positive charge in azupyrenium monocation **2aH**$^+$ is extensively delocalized throughout the system, changes in the computed $\Delta\delta^{13}$C value at C-7/C-8/C-10 and C-10c are rather small. For **2aH$_2$**$^{2+}$, positive charge is delocalized throughout the periphery except for the inner C(10b) and C(10c) positions which carry little positive charge. Azupyrene dication **2**$^{2+}$ exhibits extensive charge delocalization, with C(2a)/C(10a)/C(5a)/C(7a) and C(4)/C(9) positions showing the largest $\Delta\delta^{13}$C values. Similar overall patterns may be derived based on changes in NPA-derived charges in these species.

The computed NICS and ΔNICS values for azupyrene cations are gathered in Fig. 8. Only the five-membered ring in **2aH**$^+$ is aromatic. In contrast, the five-membered ring in **2aH$_2$**$^{2+}$ is anti-

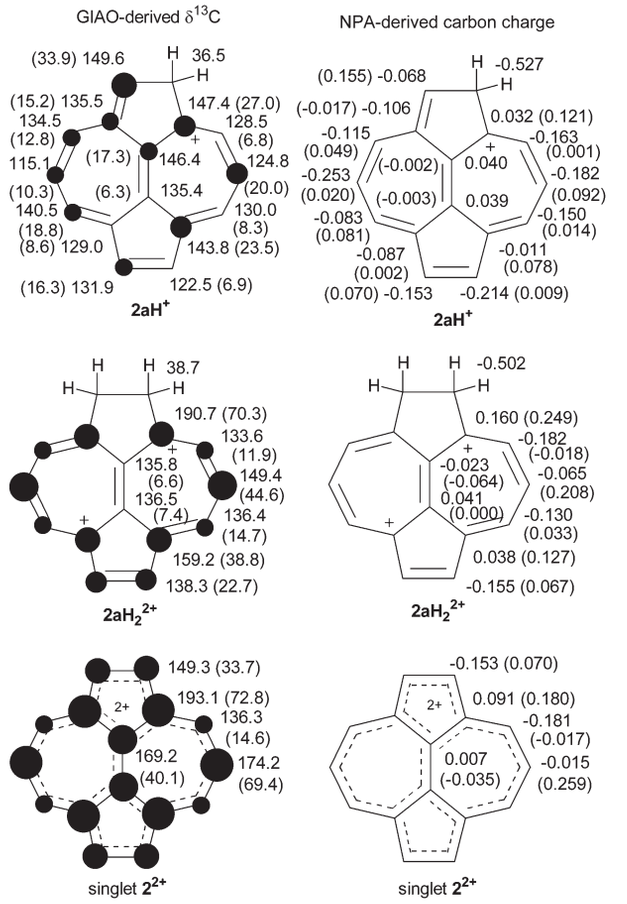

Fig. 7 Computed ^{13}C NMR chemical shifts, NPA-derived carbon charges, and NPA-derived overall charges over CH units for **2aH**$^+$, **2bH**$_2^{2+}$, **2**$^{2+}$ ($\Delta\delta^{13}$C values and Δcharges relative to **2** in parentheses). [Dark circles are roughly proportional to the magnitude of $\Delta\delta^{13}$C values; threshold was set to 10 ppm].

aromatic and the tropylium moieties are borderline-aromatic. As found for **1**$^{2+}$, the singlet azupyrene dication is antiaromatic and should be paratropic, but the less stable triplet **2**$^{2+}$ dication is predicted to be aromatic.

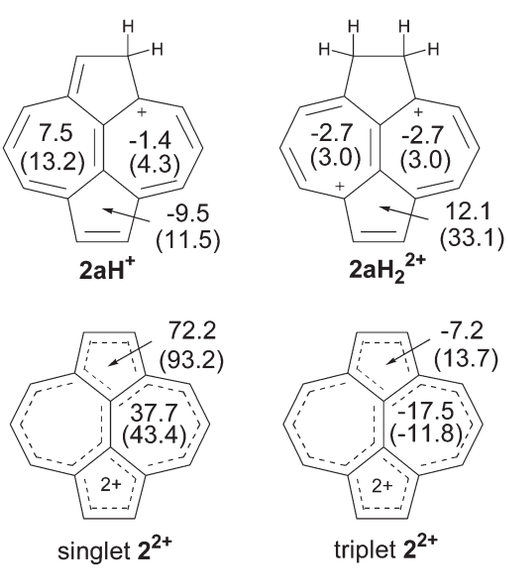

Fig. 8 NICS(0) for **2**aH$^+$, **2bH**$_2^{2+}$ and the singlet and triplet **2**$^{2+}$ (ΔNICS values relative to those of **2** in parentheses).

Optimized structures for **2**, **2aH**$^+$, **2aH**$_2^{2+}$ and **2**$^{2+}$ and the computed bond-lengths are shown in Fig S8 for comparison. The X-ray structural data on **2** are also included for comparison (Fig S9). Overall, the reported bond-lengths from the X-ray data[6] are shorter than the computed values and the differences are in some cases rather noticeable. To examine the effect of basis set, structure optimization on **2** was performed at the augmented B3LYP/6-311 ++ G(d,p) level. This reduced the differences between the computed values and the reported X-ray data, but there were still notable differences. For further comparison, structure optimization on **2** was performed at the HF/6-31G(d) level (Fig S9). This resulted in slightly shorter bonds relative to the DFT results. Thus the structural feature of a (14) annulene perturbed by a distinctly short central double-bond is not well reproduced by theory. However, this feature can be inferred by considering the optimized geometries of the azupyrenium cations **2aH**$^+$, **2aH**$_2^{2+}$ and **2**$^{2+}$ which exhibit clear bond-alternation throughout the periphery but exhibit almost no change in the central double-bond, indicating that there is little conjugation with the peripheral π-bonds.

Dicyclohepta[*ed*,*gh*]pentalene (3). The DFT optimized structures of **3** with C_s symmetry (this geometry is almost the same as the D_{2h} symmetrical structure), **3cH**$^+$ (protonation at C-5) with C_s symmetry, and **3eH**$_2^{2+}$ (di-protonation at C-5 and C-10) with C_s symmetry were calculated to be the lowest energy minima (see Fig. 9, Fig. S10 and Table S1 of the ESI). Optimization with higher symmetrical restriction (D_{2h}) gave the same structures. Protonation at C(5) (5-membered ring) (**3cH**$^+$) is strongly favored over attack at C(1) or C(2) (7-membered ring). Protonation at the central double-bond (**3dH**$^+$) lies 17 kcal mol^{-1} higher in energy relative to **3cH**$^+$ and seems highly unlikely. The lowest energy dication **3eH**$_2^{2+}$ results from diprotonation at C(5) and C(10).

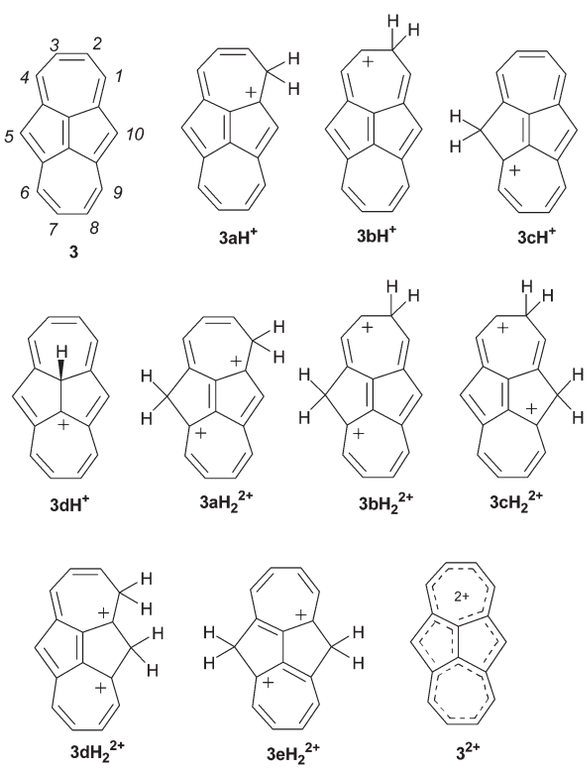

Fig. 9 Dicyclohepta[*ed*,*gh*]pentalene (**3**), protonated carbocations (**3aH**$^+$–**3dH**$^+$), diprotonated carbocations (**3aH**$_2^{2+}$–**3eH**$_2^{2+}$), and the oxidation dication (**3**$^{2+}$).

Whereas the singlet and triplet dications (**3**$^{2+}$) are both minima (C_s symmetry; this geometry is almost the same as the D_{2h} symmetrical structure), the triplet dication was computed to be 13 kcal mol^{-1} more stable.

The forms of HOMO–LUMO in the singlet and triplet **3**$^{2+}$ are illustrated in Fig. S12. The LUMO of the singlet dication has a large coefficient at the central double bond, implying that subsequent nucleophilic attack under appropriate conditions may provide a means for preparation of [14]annulenes. In triplet **3**$^{2+}$, two electrons are distributed into two SOMOs which are spread throughout the peripheral ring and delocalized into the five-membered rings.

The DFT-optimized structures of **3**, **3cH**$^+$, **3eH$_2$**$^{2+}$, and **3**$^{2+}$ and the computed bond-lengths are shown in Fig S10 for comparison. Computed bond-lengths in hydrocarbon **3** (first optimized at the B3LYP/6-31G(d) level and subsequently at the HF/6-31G(d) level for comparison) compare reasonably well with the reported X-day data[5b] (Fig S11), and the presence of a short central double-bond is clearly indicated.

Apart from lengthening of the bonds attached to the sp^3-center(s), a distinct feature in **3cH**$^+$ and **3eH$_2$**$^{2+}$ is notable lengthening of the central double bond. This feature becomes even more pronounced in the singlet **3**$^{2+}$.

Computed GIAO-NMR data and the NPA-derived charges and their respective changes for **3cH**$^+$, **3eH$_2$**$^{2+}$ and the singlet and triplet **3**$^{2+}$ are summarized in Figs. 10–11. Charge delocalization in **3cH**$^+$ resembles an azulenium ion[22] coupled to a tropylium moiety (a bis-tropylium species). Further protonation at C(10) generates a bis-azulenium dication species with largest $\Delta\delta^{13}$C values at the central double bond. In both singlet and triplet dications positive charges is strongly localized in the five-membered rings.

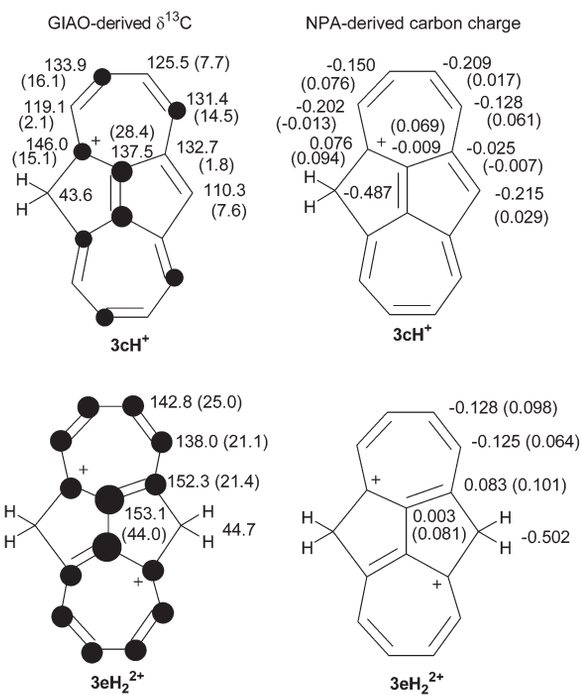

Fig. 10 Computed ^{13}C NMR chemical shifts and NPA-derived carbon charges for **3cH**$^+$ and **3eH$_2$**^{2} ($\Delta\delta^{13}$C values and Δcharges relative to **3** in parentheses). [Dark circles are roughly proportional to the magnitude of $\Delta\delta^{13}$C values; threshold was set to 10 ppm].

Based on NICS and ΔNICS (Fig. 12) the tropylium moieties in **3cH**$^+$ and **3eH$_2$**$^{2+}$ are clearly aromatic, whereas the five-membered ring is anti-aromatic. It is also noteworthy that the tropylium moiety is only aromatic in the singlet dication **3**$^{2+}$.

Comparative discussion and summary

The present DFT study has examined the mono- and dications of protonation as well as the oxidation dications of the nonalternant isomers of pyrene namely DCPH "azupyrene" **2** and DCHP **3** in comparison with pyrene **1**.

DFT concurs with previous stable ion data on the mono-protonation of **1** and enhances the previous semiempirical data. New insights have been obtained regarding the hitherto elusive diprotonated dications of **1**. The GIAO-based charge delocalization paths agree quite well with the stable ion NMR data. Paratropicity (antiaromaticity) in singlet **1**$^{2+}$ previously deduced by NMR is reaffirmed by NICS. Furthermore, NICS predicts that the less stable triplet dication should be aromatic (diatropic).

The optimized geometry of azupyrene **2** does not closely duplicate its reported X-ray structure. In line with electrophilic aromatic

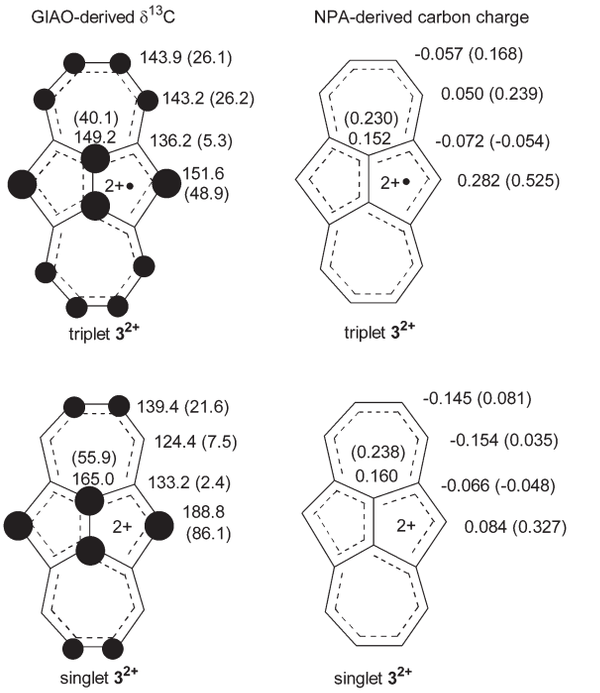

Fig. 11 Computed ^{13}C NMR chemical shifts and NPA-derived carbon charges singlet and triplet **3**$^{2+}$ ($\Delta\delta^{13}$C values and Δcharges relative to **3** in parentheses). [Dark circles are roughly proportional to the magnitude of $\Delta\delta^{13}$C values; threshold was set to 10 ppm].

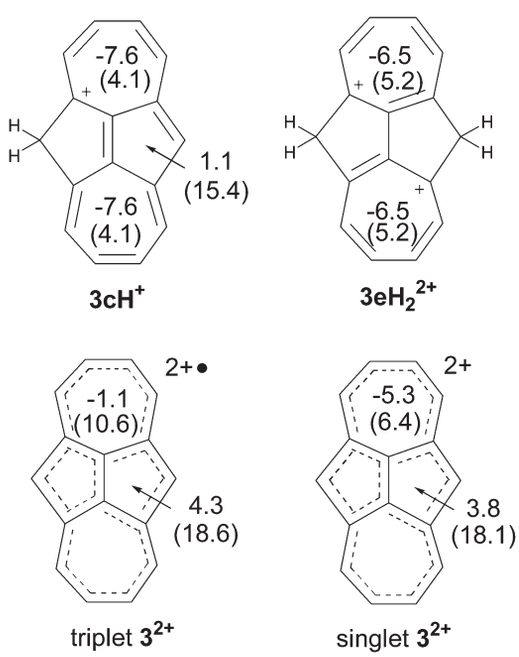

Fig. 12 NICS(0) for **3aH**$^+$, **3aH$_2$**$^{2+}$ and singlet and triplet **3**$^{2+}$ (ΔNICS values relative to those of **3** in parentheses). Based on NICS, the seven-membered rings in the triplet dication are aromatic whereas they are nonaromatic in the triplet species.

substitution data on **2**, the carbocation resulting from attack at the 5-membered ring has the lowest energy. Attack at the seven-membered ring is possible but less preferred. Charge delocalization in the lowest energy monocation, is that of a tropylium cation. The same ring preferentially undergoes further protonation to generate a bis-tropylium dication moiety. Based on NICS, the five-membered ring is aromatic in the monocation and antiaromatic in the dication. The singlet and triplet dications of **2** are both minima and the triplet lies only is 4 kcal mol^{-1} higher. In comparison, the triplet state in **1**$^{2+}$ is 14.6 kcal mol^{-1} higher in energy. As deduced for **1**$^{2+}$, the triplet **2**$^{2+}$ is clearly aromatic whereas the lower energy singlet **2**$^{2+}$ is antiaromatic (paratropic). The central double bonds in singlet **1**$^{2+}$ and **2**$^{2+}$ do not contribute to HOMO.

The DFT-optimized structure of **3** matches closely its reported X-ray structure. The electrophilic chemistry of **3** is clearly controlled by the five-membered rings. Thus mono- and diprotonations are directed to these sites. Charge delocalization pattern in the monocation resembles an azulenium cation coupled to a tropylium moiety, whereas the delocaliztion path in the dication resembles a bis-azulenium species. Although, as in previous cases, the singlet and triplet dication of **3** are both minima, in this case the triplet dication is 13 kcal mol^{-1} more stable. Positive charge in the dications is strongly localized on the five-membered rings. The LUMO of the singlet $\mathbf{3}^{2+}$ has a large coefficient at the central double bond, suggesting that nucleophilic addition could generate [14]annulenes.

The present computational study serves as a starting point for our planned chemical, toxicological and stable ion studies on **2** and **3**.

Acknowledgements

This work was supported in part by the NCI of NIH (NCI 2 R15 CA078235-02A1), by a grant-in-Aid for Young Scientists (B) 15710160 from the Japan Society for the Promotion of Science (JSPS), and by 21st century COE program, COE for United Approach to New Materials Science (COE program of the Ministry of Education, Culture, Sports, Science and Technology, Japan).

References

1 M. A. Quilliam, F. Messier, C. Lu, P. A. Andrews, B. E. McCarry and D. R. McCalla in *Polynuclear Aromatic Hydrocarbons, Phys. Biol. Chem., 6th Int. Symp.*, ed. M. Cook, A. J. Dennis and G. L. Fisher, Battle Press, Columbus, OH, 1982, pp. 667–672; Y.-H. Chae, B.-Y. Ji, J.-M. Lin, P. P. Fu, B. P. Cho and K. El-Bayoumy, *Chem. Res. Toxicol.*, 1999, **12**, 180; P. Upadhyaya, L. S. Von Tungeln, P. P. Fu and K. El-Bayoumy, *Chem. Res. Toxicol.*, 1994, **7**, 690.

2 See for example: J. Krzeminski, J.-M. Lin, S. Amin and S. S. Hecht, *Chem. Res. Toxicol.*, 1994, **7**, 125; A. Kaufman-Katz, H. L. Carrell and J. P. Glusker, *Carcinogenesis*, 1998, **19**, 1641; E. L. Cavalieri, S. Higginbotham, N. V. S. RamaKrishna, P. D. Devanesan, R. Todorovic, E. G. Rogan and S. Salmasi, *Carcinogenesis*, 1991, **12**, 1939.

3 A. G. Anderson, Jr., A. A. McDonald and A. F. Montana, *J. Am. Chem. Soc.*, 1968, **90**, 2993; A. G. Anderson, Jr., A. F. Montana and A. A. McDonald, *J. Org. Chem.*, 1973, **38**, 1445; A. G. Anderson, Jr., G. M. Masada and A. F. Montana, *J. Org. Chem.*, 1973, **38**, 1439.

4 A. G. Anderson, Jr., *Trends in Organic Chemistry*, 1992, **3**, 315.

5 (*a*) H. Reel and E. Vogel, *Angew. Chem. Int. Ed. Engl.*, 1972, **11**, 1013; (*b*) E. Vogel, H. Wieland, L. Schmalstieg and J. Lex, *Angew. Chem. Int. Ed. Engl.*, 1984, **23**, 717.

6 A. G. Anderson, Jr., S. C. Critchlow, L. C. Andrews and R. D. Haddock, *Acta. Crystallogr., Sect. C*, 1990, **C46**, 439.

7 C. J. Jutz and E. Schweiger, *Synthesis*, 1974, 193.

8 K. Hafner, H. Diehl and W. Richarz, *Angew. Chem.*, 1976, **4**, 125.

9 A. G. Anderson, Jr., E. R. Davidson, E. D. Daugs, L. G. Kao, R. L. Lindquist and K. A. Quenemoen, *J. Am. Chem. Soc.*, 1985, **107**, 1896.

10 J. Alexander, M. Baumgarten, K.-U. Klabunde and K. Müllen, *Tetrahedron Lett.*, 1991, **32**, 735.

11 (*a*) K. K. Laali, *Chem. Rev.*, 1996, **96**, 1873; (*b*) K. K. Laali and T. Okazaki, *Annu. Rep. NMR Spectrosc.*, 2002, **47**, 149–214.

12 K. K. Laali and P. E. Hansen, *J. Org. Chem.*, 1991, **56**, 6795; K. K. Laali and P. E. Hansen, *J. Org. Chem.*, 1993, **58**, 4096; K. K. Laali and P. E. Hansen, *J. Chem. Soc. Perkin. Trans 2*, 1994, 2249; K. K. Laali and P. E. Hansen, *Res. Chem. Intermed.*, 1996, **22**, 737.

13 K. K. Laali, P. E. Hansen, E. Gelerinter and J. J. Houser, *J. Org. Chem.*, 1993, **58**, 4088.

14 K. K. Laali, M. Tanaka and P. E. Hansen, *J. Org. Chem.*, 1998, **63**, 8217.

15 See for example: (*a*) K.-M. Li, M. George, M. L. Gross, C.-H. Lin, R. Jankowiak, G. J. Small, A. Seidel, H. Kroth, E. G. Rogan and E. L. Cavalieri, *Chem. Res. Toxicol.*, 1990, **12**, 778; (*b*) V. J. Melendez-Colon, A. Luch, A. Seidel and W. M. Baird, *Chem. Res. Toxicol.*, 2000, **13**, 10; (*c*) M. K. Lakshman, F. N. Ngassa, S. Bae, D. G. Buchanan, H.-G. Hahn and H. Mah, *J. Org. Chem.*, 2003, **68**, 6020.

16 T. Okazaki, K. K. Laali, B. Zajc, M. K. Lakshman, S. Kumar, W. M. Baird and W.-M. Dashwood, *Org. Biomol. Chem.*, 2003, **1**, 1509.

17 R. G. Harvey and N. E. Geacintov, *Acc. Chem. Res.*, 1988, **21**, 66.

18 *Gaussian 98*, Revision A.9, M. J. Frisch, G. W. Trucks, H. B. Schlegel, G. E. Scuseria, M. A. Robb, J. R. Cheeseman, V. G. Zakrzewski, J. A. Montgomery, Jr., R. E. Stratmann, J. C. Burant, S. Dapprich, J. M. Millam, A. D. Daniels, K. N. Kudin, M. C. Strain, O. Farkas, J. Tomasi, V. Barone, M. Cossi, R. Cammi, B. Mennucci, C. Pomelli, C. Adamo, S. Clifford, J. Ochterski, G. A. Petersson, P. Y. Ayala, Q. Cui, K. Morokuma, D. K. Malick, A. D. Rabuck, K. Raghavachari, J. B. Foresman, J. Cioslowski, J. V. Ortiz, A. G. Baboul, B. B. Stefanov, G. Liu, A. Liashenko, P. Piskorz, I. Komaromi, R. Gomperts, R. L. Martin, D. J. Fox, T. Keith, M. A. Al-Laham, C. Y. Peng, A. Nanayakkara, M. Challacombe, P. M. W. Gill, B. Johnson, W. Chen, M. W. Wong, J. L. Andres, C. Gonzalez, M. Head-Gordon, E. S. Replogle and J. A. Pople, Gaussian, Inc., Pittsburgh PA, 1998.

19 P. v. R. Schleyer, C. Maerker, A. Dransfeld, H. Jiao and N. J. v. E. Hommes, *J. Am. Chem. Soc.*, 1996, **118**, 6317.

20 K. Wolinski, J. F. Hinton and P. Pulay, *J. Am. Chem. Soc.*, 1990, **112**, 8251; R. Dichfield, *Mol. Phys.*, 1974, **27**, 789.

21 M. J. J. Dewar and R. D. Dennington, II, *J. Am. Chem. Soc.*, 1989, **111**, 3804.

22 T. Okazaki and K. K. Laali, *Org. Biomol. Chem.*, 2003, **1**, 3078.